Journal of Electroanalytical Chemistry 683 (2012) 43–46

Contents lists available at SciVerse ScienceDirect

Journal of Electroanalytical Chemistry

journal homepage: www.elsevier.com/locate/jelechem

Photocurrent enhancement in dye-sensitized photovoltaic devices with titania–graphene composite electrodes

Javier Durantini [b], Pablo P. Boix [a], Miguel Gervaldo [b], Gustavo M. Morales [b], Luis Otero [b], Juan Bisquert [a], Eva M. Barea [a,*]

[a] Photovoltaic and Optoelectronic Devices Group, Physics Department, Universitat Jaume I, 12071 Castelló, Spain
[b] Departamento de Química, Universidad Nacional de Río Cuarto, Agencia Postal Nro. 3, X5804BYA Río Cuarto, Córdoba, Argentina

ARTICLE INFO

Article history:
Received 5 June 2012
Received in revised form 20 July 2012
Accepted 24 July 2012
Available online 14 August 2012

Keywords:
Graphene
Dye solar cells
Impedance

ABSTRACT

Photovoltaic performance of dye-sensitized solar cell (DSC) devices based on a new titania–graphene paste has been investigated using Impedance Spectroscopy (IS) technique. The results provide key information about device performance, clarifying that photocurrent increment is not related to lower charge transfer resistance, neither with a downshift of the Fermi level of the graphene titania semiconductor. The DSC devices constructed using titania–graphene paste and graphene thin films reach higher photocurrent and therefore higher efficiency than devices made with a commercial paste due to extra photocurrent generation, because the titania–graphene paste presents higher light harvesting in the visible region of the solar spectra combined with large scatter effect than the commercial titania paste.

1. Introduction

Nanocrystalline semiconductor-based dye-sensitized solar cells (DSCs) have attracted significant attention as a low cost alternative to conventional solid-state photovoltaic devices [1]. The most successful dye sensitizers employed so far in these cells are polypyridyl-type ruthenium complexes [2,3] yielding overall AM 1.5 solar to electric power conversion efficiencies (PCEs) upto 11.7% [4]. Further improvements are still necessary and new materials as well as novel device fabrications need to be thoroughly explored. Several efforts are focused on improving the overall efficiency of DSCs, such as the exploration of new dyes to extend the solar irradiation absorption to the infrared and near infrared region [5–7], materials for counterelectrodes to improve charge extraction [8], new redox mediators that can get higher open circuit potential [9] and new semiconductor materials. Composite metal oxides with different bandgaps [10] have been widely studied, as well as porous structures ordered in a perpendicular fashion to the conducting substrate [11–14]

Recently, the reduced graphene oxide (rGO), one type of graphene derivative, has been extensively used for biosensors [15], memories [16], transistors [17] and in DSCs [18]. The use of graphene in the DSC increases the overall conversion efficiency, but its function in the solar cell is still under investigation because there are many functional factors that are still unclear. It was suggested that graphene can absorb molecules (hydrocarbons) [19] or atoms (hydrogen) and the defects act as a conducting channel [19]. In general, an increase of the photocurrent has been observed when using graphene in a DSC, and it should be clarified which mechanism is causing this effect that promotes the overall power conversion efficiency.

In this paper we report photoelectrochemical and Impedance Spectroscopy (IS) studies of two different sets of TiO_2-graphene DSCs, in addition to control devices. The first one consists in an active nanostructured electrode made by a mixture of titania–graphene paste fabricated by hydrothermal synthesis. In the second set a commercial titania paste is deposited onto a graphene layers deposited by spin coated on fluorine tin oxide (FTO) conducting glass. In both cases, the DSC containing graphene (composite or layered) present higher conversion efficiency than the reference device without graphene due to a large increase in the photocurrent.

2. Experimental section

2.1. Synthesis and characterization of TiO_2–graphene composite material

The synthesis method used to obtain the titania–graphene composite was based on a modification of the Kang's procedure [20] Briefly, 4 mg of graphene oxide dispersed in 12 ml of H_2O and 4 ml of glacial acetic acid were poured into a conical flask immersed into an ice bath, stirred and then allowed to cool.

* Corresponding author. Tel.: +34 964387553.
E-mail address: barea@fca.uji.es (E.M. Barea).

1572-6657/$ - see front matter © 2012 Elsevier B.V. All rights reserved.
http://dx.doi.org/10.1016/j.jelechem.2012.07.032

Afterwards, 0.45 ml of isopropanol (Aldrich, 99.5%) is added to a dropping funnel followed by 1.80 ml of titanium isopropoxide (Aldrich, 97%). The titanium isopropoxide/isopropanol solution was dripped into the acetic acid solution at a rate of approximately 1–2 drops per second with vigorous stirring. Then the mixture is kept between 4 and 8 h. Under reflux to achieve the peptisation. The obtained colloidal suspension was loaded in Teflon-lined stainless steel autoclave and heat at 200 °C for 12 h. The titania–graphene was dispersed by ultrasound for 30 s to disperse the aggregates, followed by a concentration until 13 wt% of titania nanoparticles was reached. In order to obtain the final paste, the titania graphene composite are mixed with 20 wt% polyethylene glycol (Fluka, MW 20,000) and 20 wt% polyethylene oxide (Aldrich, MW 100,000).

The titania–graphene paste were characterized by X-ray diffraction spectroscopy using D4 Endeavor, Bruker-AXS (Fig. S1 in SI), where it is clearly observed that the TiO_2 present in the composite is obtained in the anatase phase. The less intensity of the peak and the broadness is due to the defects generated in the 3-dimensional framework by the graphene flakes. In addition, graphene shows peaks close to the anatase phase of titania which broadness the XRD spectra.

All the prepared materials were characterized by Transmission Electron Microscopy (TEM) using a Philips CM200 UT microscope operating at 200 kV and room temperature and by Atomic force microscopy (AFM), that were performed using an Agilent 5500 SPM microscope (Agilent Technologies, Inc.) working in Acoustic AC Mode. Commercial silicon cantilever probes, with aluminum backside coating, and nominal tip radius of 10 nm (Mikro Masch, NSC15/Al BS/15, spring constant ranging 20–75 N m^{-1}), were employed just under their fundamental resonance frequencies of about 325 kHz. Height and phase images were acquired simultaneously under ambient conditions. Scan rates were set between 0.5 and 2 Hz depending on the size of the images. Fig. 1 shows a typical TEM and high resolution TEM image of the as synthesized titania–graphene paste. It is apparent that the composites consisted of uniform TiO_2 nanoparticles with diameters of about 15 nm grow on the graphene flakes. It is observed that both components, graphene and semiconductor TiO_2, have been integrated in an intimate interfacial contact [21].

The surface morphologies of the prepared composite electrodes were examined with AFM in order to observe their topology, Fig. S2 in SI shows a typical Acoustic AC Mode AFM height mode image of the deposited titania–graphene on FTO. No significant differences in topological features were found for the electrodes prepared by using TiO_2 with and without graphene. As can be seen, the films present a highly rough and open surface, with the presence of small features assigned to the presence of TiO_2 nanoparticles. The observed microstructure must be a consequence of the nucleation, and further TiO_2 growing process over graphene flakes in agreement with the observed in TEM images.

2.2. DSC fabrication and characterization

Two sets of electrodes, named GP (graphene paste, titania–graphene paste fabricated by hydrothermal synthesis) and GF (graphene film, commercial titania paste is deposited onto a graphene oxide layers deposited by spin coating on fluorine tin oxide (FTO) conducting glass) were prepared and sensitized with N719 dye (0.5 mM acetonitrile/tert-butanol N719 and 0.5 mM chenodeoxycholic acid 98% solution) for 24 h. Both sets were manufactured by Doctor Blade technique on FTO (Pilkington TEC15, ~15 Ω/sq resistance) or on a spin coated film of graphene oxide deposited on TCO. All the electrodes were made with two different layers of TiO_2, a transparent commercial paste and a scattering layer (commercial paste and graphene paste) calcined at 450 °C under

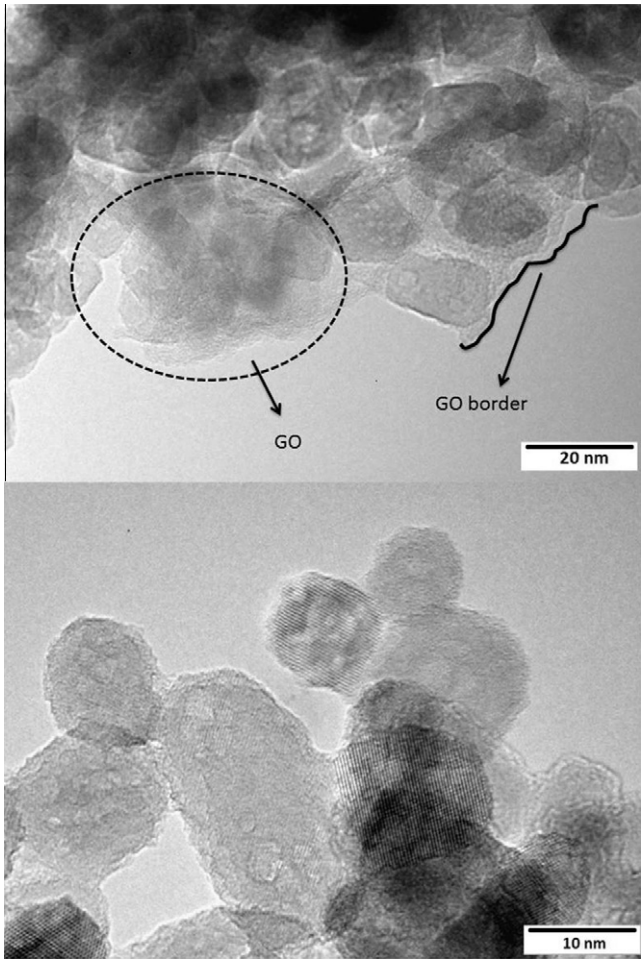

Fig. 1. TEM image of the as synthesized graphene–titania paste. GO is the graphene oxide.

N_2 atmosphere during 30 min, with a 19–20 μm thickness total. The solar cells were assembled with counter electrode thermally platinized using a thermoplastic frame (Surlyn 25 μm thick). The redox electrolyte [0.6 M methyl propyl imidazolium iodide, 0.03 M I_2 (99.9%) and 0.5 M 4-tert-butylpyridine in acetonitrile/valeronitrile (85:15)] was introduced through a hole drilled in the counter electrode that was sealed afterwards. Prepared solar cells (0.3 cm^2 size, masking solar cell to 0.25 cm^2) were characterized by current–voltage characteristics and incident photon to current efficiency (IPCE). UV/V is data was obtained using a Cary 300 Bio Spectrophotometer with the adequate setup for thin-film analysis. Photocurrent and voltage were measured using a solar simulator equipped with a 1000 W ozone-free Xenon lamp and AM 1.5 G filter (Oriel), were the light intensity was adjusted with an NREL-calibrated Si solar cell with a KG-5 filter to 1 sunlight intensity (100 mW cm^{-2}) and a 250 W Xenon arc lamp (Oriel) served as a light source for IPCE. Impedance Spectroscopy measurements (IS) were carried out under 1 sun illumination (AM 1.5 conditions) at different applied bias potentials, ranged from zero to open-circuit photovoltage, with frequencies varying between 1 MHz and 0.01 Hz.

3. Results and discussion

The current–potential (j–V) curves obtained for both sets of cells assembled with different working electrode are plotted in Fig. 2. The solar cells parameters extracted from these curves

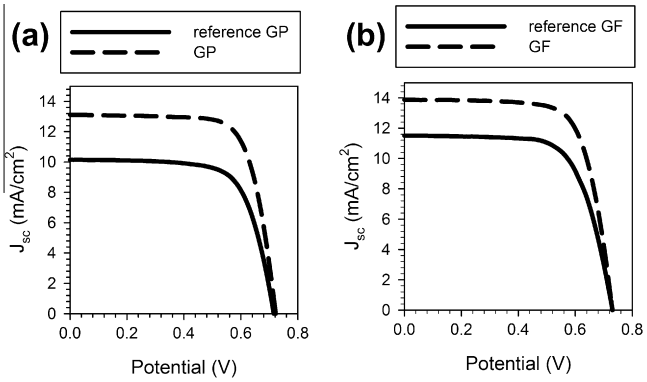

Fig. 2. *j–V* curves for DSCs prepared with (a) graphene paste (GP) and (b) graphene film (GF).

Table 1
Photovoltaic performances of DSCs fabricated with graphene and commercial paste and sensitized with N719.

DSC	V_{oc} (V)	J_{sc} (mA/cm^2)	FF	Efficiency (%)
GP	0.72	13.2	0.73	7.1
Reference for GP	0.71	10.2	0.70	5.1
GF	0.73	14.0	0.72	7.3
Reference for GF	0.73	11.6	0.70	5.8

V_{oc} is the open circuit voltage, J_{sc} is the density current, FF is the fill factor. Values are obtained at steady-state measurement under 100 mW cm^{-2} light intensity and AM 1.5 global radiation.

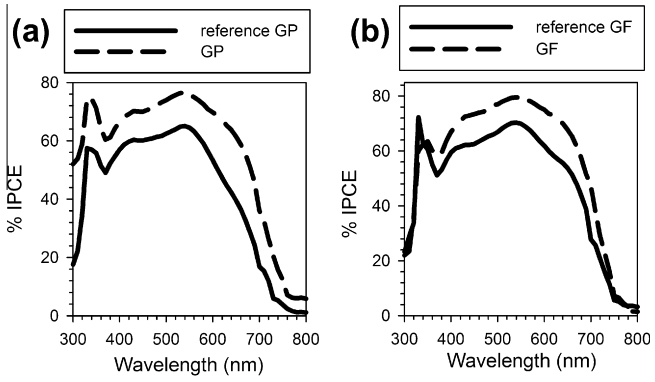

Fig. 3. IPCE for DSCs set of (a) GP and (b) GF and the references DSC.

are indicated in Table 1. Note that for sets GP and GF, the main difference is observed in the photocurrent, with an increase of 3 mA/cm^2 for the DSC with GP and 2.4 mA/cm^2 for GF DSC, that enhance the overall conversion efficiency of the cell by around 20%. The increase in the photocurrent is also observed in the incident photon-to-current conversion efficiency (IPCE) (Fig. 3).

To clarify the mechanism governing the performance of the devices IS measurements were performed on the DSCs at different bias potentials (from zero to open circuit potential, step 0.05 V) under 1 sun irradiation in a frequency range from 1 MHz to 10 mHz. These measurements were analyzed using the impedance model developed by Bisquert and co-workers [22,23], allowing to isolate the recombination resistance from other resistive contributions in the cell. The aim of IS measurements here is to identify variations in the devices concerning the changes of the rate of transport and recombination and also shift in the capacitance due to the presence of graphene that could strongly influence the performance [24]. Details about the methodology and the interpretation

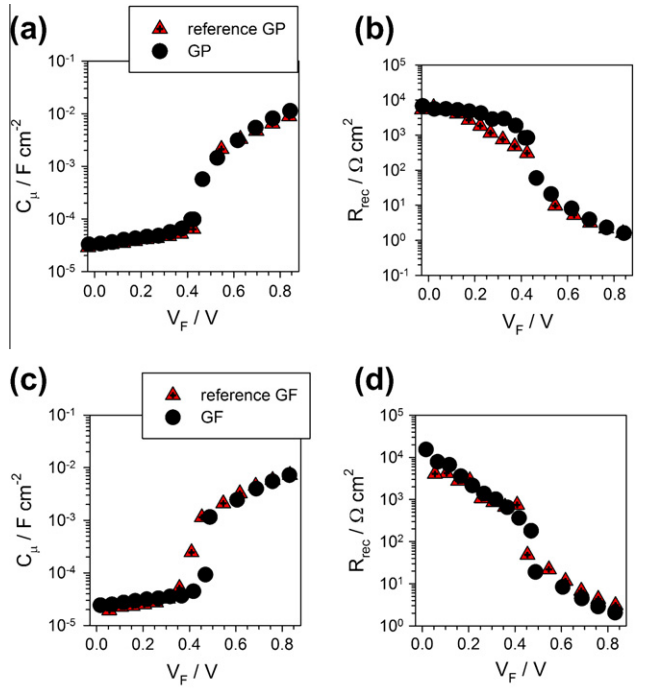

Fig. 4. (a) Capacitance and (b) recombination resistance, with respect to the Fermi level voltage (removing the effect of series resistance) for GP set of DSC. (c) Capacitance and (d) recombination resistance respect to the Fermi level voltage for GF set of DSC.

of IS results in connection to the performance of DSCs are provided in recent papers [25–29] The chemical capacitance and recombination resistance are plotted vs V_F (Femi level voltage), that corresponds to remove from the bias voltage the effect of ohmic drops in the solar cell. IS enables extracting the voltage drop in the sensitized electrode, V_F, at each applied potential, V_{app}, by subtracting the effect of the series resistance on both R_{rec} and C_μ as follows: $V_F = V_{app} - V_s - V_{ce}$, where V_s and V_{ce} are potential drops at the series resistance and at the counter-electrode, respectively. V_F is proportional to the rise of the Fermi level of electrons in TiO_2, $V_F = (E_{Fn} - E_{F0})/q$, where q is the positive elementary charge and E_{Fn} and E_{F0} are the electron quasi-Fermi level and the electron Fermi level at the equilibrium.

Fig. 4 shows a similar chemical capacitance and recombination resistance in both set of samples, with and without graphene. This clearly indicates that graphene does not shift the conduction band of TiO_2 and neither influences the recombination process. The electron conductivity in the semiconductor, usually measured by the reciprocal of the transport resistance, was too large to be measured, being the transport resistance negligible in both sets of samples (GP and GF). This indicates that the current limitation in the case of commercial titania DSC is not due to low transport rate in TiO_2 [27].

The interpretation of IS measurements therefore shows that a number of features usually employed to explain the increase in the photocurrent in DSC can be ruled out in the present investigation, namely: lower recombination rate, a down shift of the capacitance that could increase the injection from the LUMO level of the dye, or larger electron conductivity. Therefore, the increase in the photocurrent and its associated increase in the efficiency could be related to a combination of two factors. (1) Increase in the light harvesting from 400 nm to 800 nm [30] due to the scatter effect by presence of graphene flakes (Fig. 5), combined with an increase in the absorption compared with the reference titania commercial paste (Fig. 6). (2) Extra electron injection under illumination from

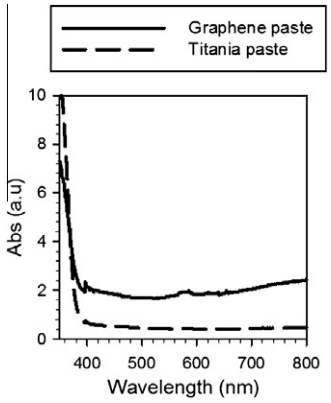

Fig. 5. *UV–vis* spectra of the naked titania films made by commercial titania paste and graphene paste.

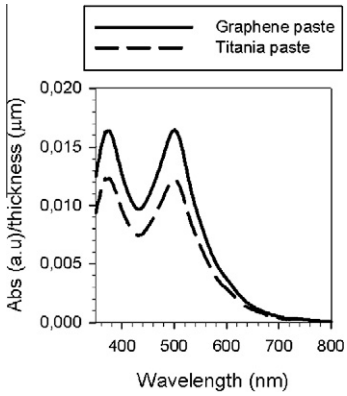

Fig. 6. *UV–vis* spectra normalized to thickness films for the sensitized graphene based electrode and commercial paste based electrode.

the graphene in the composite and from the graphene film, due to the fact that the extra electrons of six-membered ring concentrate in the LUMO level [31], also because the defects of the graphene act as a conducting channel [19], or some plasmon effect that cannot be rule out and has been reported recently in the bibliography [32,33]. Our results therefore show that the extra current obtained in DSC made with GP or GF is due to the nature of graphene, its light absorption and scattering properties in the visible region. As a consequence, this work opens a new path in the improvement of the DSC, in particular an increase of photocurrent using titania–graphene composites.

4. Conclusions

In summary, graphene is a material of general interest for optoelectronic devices, and we introduced it into the working electrode of DSC successfully. The short-circuit current density and the conversion efficiency of the DSC was increased. The enhancement of the light harvesting and higher scatter effect of the naked graphene titania paste is what generate extra photocurrent without any energetic and structural change in the semiconductor. This is confirmed by impedance spectroscopy results that show the same recombination resistance and no downshift of the conduction band of titania.

Acknowledgments

We acknowledge support by projects from Ministerio de Economia y Competitividad of Spain (Consolider HOPE CSD2007-00007, MAT2010-19827), and GeneralitatValenciana (PROMETEO/2009/058 and the "Institute of Nanotechnologies for Clean Energies"ISIC/2012/008.).Red Cyted - Red Temática 5511RT0416. The SCIC of University Jaume I (Spain) for providing the XRD facilities and M.S. Moreno, Centro AtómicoBariloche, by the TEM images.

Appendix A. Supplementary material

Supplementary data associated with this article can be found, in the online version, at http://dx.doi.org/10.1016/j.jelechem.2012.07.032.

References

[1] B. ÓRegan, M. Grätzel, Nature 353 (1991) 737.
[2] A. Kay, M.K. Nazeeruddin, I. Rodicio, R. Humphry-Baker, E. Muller, P. Linska, N. Vlachopoulus, M. Grätzel, J. Am. Chem. Soc. 115 (1993) 6382–6390.
[3] P. Pechy, M.K. Nazeeruddin, O. Kohle, S.M. Zakeeruddin, R. Humphry-Baker, M. Grätzel, J. Am. Chem. Soc. 65 (1995).
[4] Q. Yu, Y. Wang, Z. Yi, N. Zu, J. Zhang, M. Zhang, P. Wang, ACS Nano. 4 (10) (2010) 6032–6038.
[5] A. Mishra, M.K.R. Fischer, P. Bäuerle, Angew. Chem. Int. Ed. 48 (2009) 2474.
[6] M. Gratzel, Acc. Chem. Res. 42 (2009) 1788.
[7] M. Pastore, P. De Angelis, ACS Nano 4 (2010) 556.
[8] R. Trevisan, M. Döbbelin, P.P. Boix, E.M. Barea, T. Tena-Zaera, I. Mora-Seró, J. Bisquert, Adv. Energy Mater. 1 (2011) 781–784.
[9] X. Mingfei, Z. Difei, C. Ning, L. Jingyuan, L. Renzhi, W. Peng, Energy Environ. Sci. (2011), http://dx.doi.org/10.1039/c1ee02432a.
[10] F.T. Kong, S.Y. Dai, K.J.R. Wang, Adv. Optoelectron. (2007) 1–13.
[11] D.B. Kuang, J. Brillet, P. Chen, M. Takata, S. Uchida, H. Miura, K. Sumioka, S.M. Zakeeruddin, M. Grätzel, ACS Nano 2 (2008) 1113–1116.
[12] A. Kongkanand, R. Martinez-Dominguez, P.V. Kamat, Nano Lett. 7 (2007) 676–680.
[13] P. Brown, K. Takechi, P.V. Kamat, J. Phys. Chem. C 112 (2008) 4776–4782.
[14] C.Y. Yen, Y.F. Lin, S.H. Liao, C.C. Weng, C.C. Huang, Y.H. Hsiao, C.C.M. Ma, M.C. Chang, H. Shao, M.C. Tsai, Nanotechnology 19 (2008) 1–9.
[15] Q.Y. He, H.G. Sudibya, Z.Y. Yin, S.X. Wu, H. Li, F. Boey, W. Huang, P. Chen, H. Zhang, ACS Nano 4 (2010) 3201.
[16] J.Q. Liu, Z.Y. Yin, X.H. Cao, F. Zhao, A. Ling, L.H. Xie, Q.L. Fan, F. Boey, H. Zhang, W. Huang, ACS Nano 4 (2010) 3987.
[17] B. Li, X.H. Cao, H.G. Ong, J.W. Cheah, X.Z. Zhou, Z.Y. Yin, H. Li, J.L. Wang, F. Boey, W. Huang, H. Zhang, Adv. Mater. 22 (2010) 3058.
[18] N. Yang, J. Zhai, D. Wang, Y. Chen, L. Jiang, ACS Nano 4 (2) (2010) 887–889.
[19] N.M.R. Peres, Rev. Mod. Phys. 82 (2010) 2673–2700.
[20] M.G. Kang, N.G. Park, Y.J. Park, K.S. Ryu, S.H. Chang, Sol. Energy Mater. Sol. Cells 75 (2003) 475–479.
[21] Y. Zhang, Z.R. Tang, X. Fu, Y.-J. Xu, ACS Nano 5 (9) (2011) 7426–7435.
[22] J. Bisquert, J. Phys. Chem. B 106 (2002) 325.
[23] F. Fabregat-Santiago, J. Bisquert, E. Palomares, L. Otero, D. Kuang, S. Zakeeruddin, M.J. Gratzel, Phys. Chem. C 111 (2007) 6550.
[24] B. O'Regan, J. Durrant, R. Acc. Chem. Res. 42 (2009) 1799.
[25] E.M. Barea, J. Ortiz, F.J. Payá, F. Fernández-Lázaro, F. Fabregat Santiago, A. Sastre-Santos, J. Bisquert, Energy Environ. Sci. 3 (2010) 1985.
[26] E. Barea, C. Zafer, B. Gultekin, B. Aydin, S. Koyuncu, S. Icli, F. Fabregat Santiago, J. Bisquert, J. Phys. Chem. C 114 (2010) 19840.
[27] F. Fabregat-Santiago, G. Garcia-Belmonte, I. Mora-Seró, J. Bisquert, Phys. Chem. Chem. Phys. 13 (2011) 9083–9118.
[28] E.M. Barea, R. Caballero, F. Fabregat-Santiago, P. de la Cruz, F. Langa, J. Bisquert, Chem. Phys. Chem. 11 (2010) 245.
[29] E.M. Barea, V. Gónzalez-Pedro, T. Ripollés-Sanchis, H.-P. Wu, L.-L. Li, C.-Y. Yeh, E.W.-G. Diau, J. Bisquert, J. Phys. Chem. C 115 (2011) 10898–10902.
[30] G. Yang, J. Zhang, P. Wang, Q. Sun, J. Zheng, Y. Zhu, Curr. Appl. Phys. 11 (2011) 376–381.
[31] S. Zhang, Y. Zhang, S. Huang, H. Liu, P. Wang, H. Tian, J. Phys. Chem. C 114 (2010) 19284–19288.
[32] P. Tassin, T. Koschny, M. Kafesaki, C.M. Soukoulis, Nat. Photon. 6 (2012) 259–264.
[33] B. Li, T. Liu, Y. Wang, Z. Wang, J. Colloid Interface Sci. 377 (2012) 114–121.